STRUCTURAL BIOLOGY COMMUNICATIONS

ISSN 2053-230X

Crystal structure of the inhibitor-free form of the serine protease kallikrein-4

Blake T. Riley,[a] David E. Hoke,[a] Sheena McGowan[b] and Ashley M. Buckle[a]*

[a]Biomedicine Discovery Institute and Department of Biochemistry and Molecular Biology, Monash University, 23 Innovation Walk, Clayton, VIC 3800, Australia, and [b]Biomedicine Discovery Institute and Department of Microbiology, Monash University, 19 Innovation Walk, Clayton, VIC 3800, Australia. *Correspondence e-mail: ashley.buckle@monash.edu

Received 8 March 2019
Accepted 4 July 2019

Edited by N. Sträter, University of Leipzig, Germany

Keywords: kallikrein-related peptidase 4; KLK4; apo structure; unliganded.

PDB reference: apo KLK4, 6nvb

Supporting information: this article has supporting information at journals.iucr.org/f

Kallikrein 4 (KLK4) is a serine protease that is predominantly expressed in the prostate and is overexpressed in prostate cancer. As such, it has gained attention as an attractive target for prostate cancer therapeutics. Currently, only liganded structures of KLK4 exist in the Protein Data Bank. Until now, inferences about the subtle structural changes in KLK4 upon ligand binding have been made by comparison to other liganded forms, rather than to an apo form. In this study, an inhibitor-free form of KLK4 was crystallized. The crystals obtained belonged to space group $P1$, contained four molecules in the asymmetric unit and diffracted to 1.64 Å resolution. Interestingly, a nonstandard rotamer of the specificity-determining residue Asp189 was observed in all chains. This model will provide a useful unliganded structure for the future structure-guided design of KLK4 inhibitors.

1. Introduction

Kallikrein-related peptidase 4 (KLK4) is a secreted serine protease under androgenic regulation (Nelson *et al.*, 1999; Yousef *et al.*, 1999). It is normally expressed in the prostate, where it plays a role in a protease cascade leading to semen liquefaction (Prassas *et al.*, 2015). Significantly, overexpression of KLK4 in the prostate is associated with both androgen-dependent and androgen-independent prostate cancers (Nelson *et al.*, 1999; Yousef *et al.*, 1999; Ramsay *et al.*, 2008). As a result, KLK4 has come into view as an emerging target for prostate cancer therapeutics (Prassas *et al.*, 2015).

As a serine protease target, standard-mechanism inhibitors have been developed against KLK4. By grafting optimal substrates into cyclopeptide inhibitor scaffolds, potent, selective inhibitors against KLK4 have been designed (Swedberg *et al.*, 2009, 2011, 2018). Subsequent crystallographic studies have explored the engineered interactions between these inhibitors and KLK4 (Riley *et al.*, 2016). In the prostate, the proteolytic activity of KLK4 is suppressed by a millimolar concentration of Zn^{2+} ions. These Zn^{2+} ions bind at an allosteric site between the 70–80 loop and the N-terminal strand, and disrupt the active site of the protease (Debela, Magdolen, Grimminger *et al.*, 2006). Further structural perturbations at the active site were echoed in a crystal of KLK4 bound to Ni^{2+} (Riley *et al.*, 2016).

Understanding the subtle structural changes induced upon the binding of a ligand is strongly aided by comparison to an uninhibited structure. Currently, all eight structures of KLK4 in the Protein Data Bank (PDB) are complexed with a known inhibitor. Specifically, structures exist for KLK4 bound to

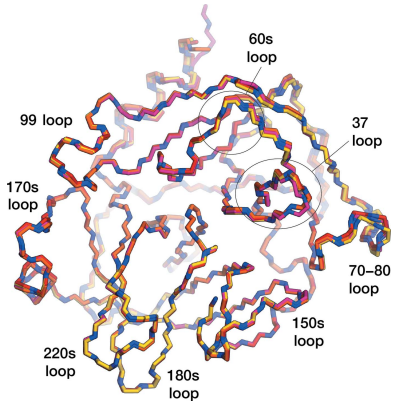

Table 1
Macromolecule-production information.

Source organism	*Homo sapiens*
Expression vector	pET12-proPSA-hK4 (Takayama *et al.*, 2001)
Expression host	*E. coli* BL21(DE3) pLysS
Complete amino-acid sequence of the construct produced†	*MAPLILSR*↓IINGEDCSPHSQPWQAALVMEN ELFCSGVLVHPQWVLSAAHCFQNSYTIGL GLHSLEADQEPGSQMVEASLSVRHPEYNR PLLANDLMLIKLDESVSESDTIRSISIAS QCPTAGNSCLVSGWGLLANGRMPTVLQCV NVSVVSEEVCSKLYDPLYHPSMFCAGGGQ DQKDSCNGDSGGPLICNGYLQGLVSFGKA PCGQVGVPGVYTNLCKFTEWIEKTVQAS

† The KLK3 propeptide is shown in italics and is autolytically cleaved at ↓ by KLK4.

SFTI-1 analogues at the active site (PDB entries 4k1e, 4k8y, 4kel and 6o21; Riley *et al.*, 2016, 2019); bound to Ni^{2+} at the active site (PDB entry 4kga; Riley *et al.*, 2016); and bound to a *p*-aminobenzamidine inhibitor at the active site and Ni^{2+}, Zn^{2+} and Co^{2+} at an allosteric regulatory site, respectively (PDB entries 2bdg, 2bdh and 2bdi; Debela, Magdolen, Grimminger *et al.*, 2006). The metal ions bind to the allosteric site between His25 on the N-terminal strand and Glu77 within the 70–80 loop, disrupting the active site of the protease and explaining why the proteolytic activity of KLK4 is suppressed by a millimolar concentration of Zn^{2+} ions (Debela, Magdolen, Grimminger *et al.*, 2006).

To aid both rational, structure-guided design of new inhibitors and future analyses of KLK4 inhibition, in this study we sought to crystallize and solve the structure of inhibitor-free KLK4.

2. Materials and methods

2.1. Macromolecule production

The previously reported pET12-proPSA-hK4 chimera plasmid (Takayama *et al.*, 2001) encodes the peptidase domain of human KLK4 (Q9Y5K2-1), including the benign, non-synonymous single-nucleotide polymophism His197Gln (VAR_028365). In this construct, the propeptide of KLK4 is replaced by the propeptide of KLK3, enabling auto-activation. This construct was transformed into *Escherichia coli* BL21(DE3) pLysS cells (Table 1), expressed into inclusion bodies and refolded and purified as described previously (Riley *et al.*, 2016).

2.2. Crystallization

The crystallization conditions for KLK4 in complex with SFTI-1 were used as a guide for crystallizing inhibitor-free KLK4. Hanging-drop vapour-diffusion crystal trays were set up manually using a 500 µl well volume and mixing 1 µl well buffer with 1 µl protein solution. Crystallization trials used 1 *M* lithium sulfate, 0.5 *M* sodium acetate and scanned 10–30%(*v*/*v*) PEG 8000, pH 4.5–6.0 and protein solution at 6, 9 and 12 mg ml^{-1}. Crystals formed as plates after a week of incubation at 293 K using the conditions given in Table 2.

Table 2
Crystallization.

Method	Vapour diffusion
Plate type	24-well, hanging drop
Temperature (K)	293
Protein concentration (mg ml^{-1})	9
Buffer composition of protein solution	50 m*M* Tris–HCl pH 7.5, 20 m*M* NaCl, 2 m*M* $CaCl_2$
Composition of reservoir solution	0.2 *M* $LiSO_4$, 0.1 *M* sodium acetate, 22% PEG 8000 pH 4.5
Volume and ratio of drop	2 µl (1 µl protein solution + 1 µl reservoir solution)
Volume of reservoir (µl)	500

Table 3
Data collection and processing.

Values in parentheses are for the outer shell.

Diffraction source	MX1, Australian Synchrotron
Wavelength (Å)	0.9537
Temperature (K)	100
Detector	ADSC Quantum 210r
Crystal-to-detector distance (mm)	149.99
Rotation range per image (°)	0.5
Total rotation range (°)	360
Exposure time per image (s)	0.5
Space group	*P*1
a, *b*, *c* (Å)	51.60, 65.72, 74.19
α, β, γ (°)	79.01, 72.91, 77.62
Mosaicity (°)	0.2
Resolution range (Å)	35.8–1.636 (1.695–1.636)
Total No. of reflections	419222 (39545)
No. of unique reflections	107669 (10360)
Completeness (%)	96.78 (93.42)
Multiplicity	3.9 (3.8)
$\langle I/\sigma(I)\rangle$	17.81 (2.09)
$R_{\rm r.i.m.}$	0.07355 (0.7973)
Overall *B* factor from Wilson plot† (Å^2)	15.75

† Ice ring in shell with resolution = 3.90 Å, $I_{\rm mean}$ = 2918.85, *Z*-score = 4.05, completeness = 0.98, average completeness = 0.99.

2.3. Data collection and processing

Crystals were transferred to a nylon loop (Hampton Research, California, USA) and cryoprotected by transferring them into mother liquor with 20%(*v*/*v*) glycerol before flash-cooling them in liquid nitrogen. Data were then collected at 100 K (nitrogen vapour stream) on the MX1 beamline at the Australian Synchrotron (Cowieson *et al.*, 2015) using the *Blu-Ice* interface (McPhillips *et al.*, 2002). Diffraction data were indexed and integrated with *XDS* (Kabsch, 2010) and scaled with *AIMLESS* (Winn *et al.*, 2011). Statistics are shown in Table 3.

2.4. Structure solution and refinement

The structure of inhibitor-free KLK4 was solved by molecular replacement with *Phaser* (McCoy *et al.*, 2007) using PDB entry 4k8y (Riley *et al.*, 2016) as a search model after removing solvent molecules and ligands. Models were then built in *Coot* (Emsley *et al.*, 2010) and refined using *PHENIX* (Adams *et al.*, 2010). Statistics for the structure refinement are presented in Table 4. Atomic coordinates and structure factors have been deposited in the Protein Data Bank with PDB accession code 6nvb and raw diffraction images are available at https://store.erc.monash.edu/experiment/view/9862/.

3. Results and discussion

In this study, the structure of an inhibitor-free form of KLK4 was successfully solved to 1.64 Å resolution, enabling the modelling of all side chains. The KLK4 protein was over-expressed in *E. coli*, purified from inclusion bodies using a previously described refolding protocol (Riley *et al.*, 2016) and crystallized. The crystals obtained belonged to space group *P*1, contained four molecules in the asymmetric unit and diffracted to 1.64 Å resolution. The structure of inhibitor-free KLK4 was determined and refined at a resolution of 1.64 Å, with an R_{work} of 15.4% and an R_{free} of 18.0% (Table 4). The structure showed the typical serine protease fold for KLK4, with an r.m.s.d. of 0.37 Å over 222 C^{α} atoms compared with PDB entry 4k8y (Riley *et al.*, 2016). Within the inhibitor-free structure all chains show good structural agreement, with all-atom r.m.s.d.s within the range 0.72–0.83 Å and C^{α} r.m.s.d.s of between 0.27 and 0.37 Å (Fig. 1). The largest differences between chains occur within the 30s loop and the 70–80 loop, reflecting the dynamic nature of these regions, as was noted in molecular-dynamics simulations of KLK4 (Riley *et al.*, 2016), although all chains of inhibitor-free KLK4 also displayed strong, continuous density for the backbone of the 70–80 loop and side chains could be modelled.

In the inhibited KLK4 crystal structures in the PDB, Asp189 occupies a **t**0 rotamer, pointing towards a *P*1 residue (here, we adopt the *Coot*/*MolProbity* rotamer nomenclature detailed in Lovell *et al.*, 2000). In our inhibitor-free structure, Asp189 occupies a drastically different rotamer to all other KLK4 structures (Fig. 2). A glycerol molecule, used as a cryoprotectant in this experiment, could be modelled in the S1 pocket which occludes the **t**0 rotamer (Fig. 3). Asp189 in all chains of our inhibitor-free structure makes a hydrogen bond to Gly185 N and instead adopts an **m**-80 rotamer (**m**-20 is the most commonly observed rotamer of Asp). The chemical environment within the deep S1 pockets is somewhat distinct from that close to bulk solvent, and the pK_a values of residues can differ substantially from the expected values (for Asp, this is 3.8). In general, where there is a cationic ligand/side chain present in the S1 pocket, the pK_a of Asp189 is predicted by *PROPKA*3.0 (Olsson *et al.*, 2011) to be around 3.6, supporting the expected deprotonation of Asp189. However, in structures in which the S1 pocket is empty, the pK_a of Asp189 is

Table 4
Structure refinement.

Values in parentheses are for the outer shell.

Resolution range (Å)	35.8–1.636 (1.695–1.636)
Completeness (%)	96.78 (93.42)
No. of reflections, working set	102290 (9875)
No. of reflections, test set	5369 (485)
Final R_{cryst}	0.1541 (0.2494)
Final R_{free}	0.1803 (0.2700)
Cruickshank DPI	0.117
No. of non-H atoms	
Total	7845
Protein	6725
Ligand	46
Water	1074
R.m.s. deviations	
Bonds (Å)	0.007
Angles (°)	1.22
Average *B* factors (Å^2)	
Overall	21.54
Protein	19.61
Ramachandran plot	
Most favoured (%)	98.53
Allowed (%)	1.47

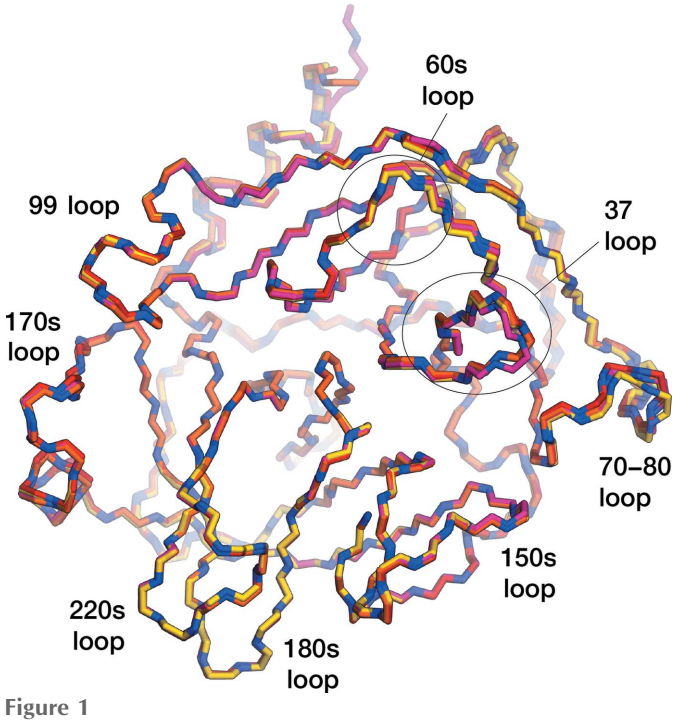

Figure 1
Overlay of the N—C^{α}—C backbone traces of all chains in the apo KLK4 structure. Chain *A* is in red, chain *B* is in orange, chain *C* is in yellow and chain *D* is in pink, with N atoms coloured blue.

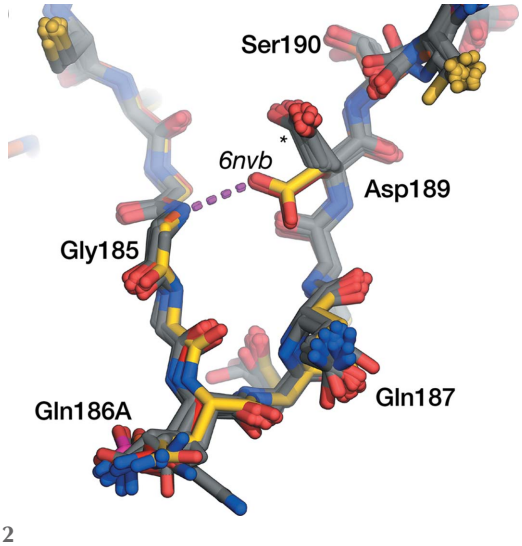

Figure 2
Overlay of crystal structures of the KLK4 S1 pocket. From PDB entry 6nvb, chain *A* is in red, chain *B* is in orange, chain *C* is in yellow and chain *D* is in pink. All other structures of KLK4 in the PDB are shown in grey. Asp189 in all chains of the apo KLK4 structure makes a hydrogen bond (magenta broken line) to Gly185 N and occupies an **m**-80 rotamer; in all other structures (marked with a star) Asp189 occupies a **t**0 rotamer, pointing upwards towards the P1 residue of a ligand.

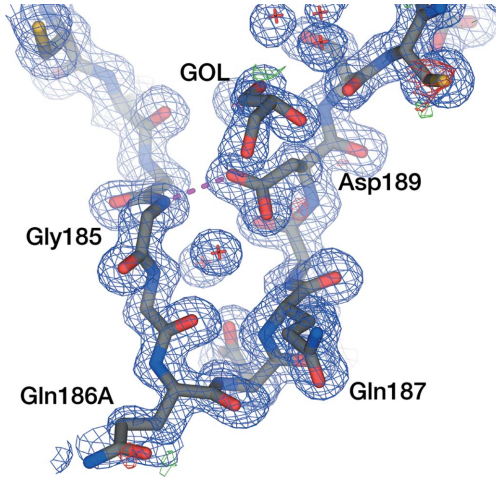

Figure 3
Electron density around Asp189 in the apo KLK4 S1 pocket. Chain *B* is shown as an exemplar. $2mF_o - DF_c$ density from a refined composite-omit map (Hodel *et al.*, 1992) contoured at 1σ is shown as a blue mesh; $mF_o \pm DF_c$ density is shown as red and green mesh contoured at -3σ and $+3\sigma$, respectively. Only residues 180–194 of the S1 pocket are shown. Asp189 makes a hydrogen bond (magenta broken line) to Gly185 N and occupies an **m**-80 rotamer; the upwards **t**0 rotamer is occluded by the presence of glycerol (GOL) in the S1 pocket.

predicted to be between 5.8 and 6.8. On the basis of this prediction, the crystallization buffer at pH 4.5 and the observed rotamer, we might tentatively infer that our crystal structure has captured a protonated Asp189 that promotes this alternative conformation.

All substrate-specificity profiling experiments have found that Arg is the preferred P1 residue of KLK4, followed by Lys (Matsumura *et al.*, 2005). This is expected as a result of Asp189 at the bottom of the S1 pocket. However, these profiling experiments also suggest that KLK4 may tolerate and be able to cleave after P1 Gly, Gln and Asn (Debela, Magdolen, Schechter *et al.*, 2006) and P1 Tyr (Borgoño *et al.*, 2007). The ability of Asp189 to adopt the observed rotamer may explain the ability of KLK4 to tolerate noncanonical, uncharged P1 residues. This structure will be useful to inform future structure-based drug design against KLK4.

Acknowledgements

This research was undertaken in part using the MX1 beamline at the Australian Synchrotron (CAP No. 11894d), which forms part of ANSTO.

References

Adams, P. D., Afonine, P. V., Bunkóczi, G., Chen, V. B., Davis, I. W., Echols, N., Headd, J. J., Hung, L.-W., Kapral, G. J., Grosse-Kunstleve, R. W., McCoy, A. J., Moriarty, N. W., Oeffner, R., Read, R. J., Richardson, D. C., Richardson, J. S., Terwilliger, T. C. & Zwart, P. H. (2010). *Acta Cryst.* D**66**, 213–221.
Borgoño, C. A., Gavigan, J.-A., Alves, J., Bowles, B., Harris, J. L., Sotiropoulou, G. & Diamandis, E. P. (2007). *Biol. Chem.* **388**, 1215–1225.
Cowieson, N. P., Aragao, D., Clift, M., Ericsson, D. J., Gee, C., Harrop, S. J., Mudie, N., Panjikar, S., Price, J. R., Riboldi-Tunnicliffe, A., Williamson, R. & Caradoc-Davies, T. (2015). *J. Synchrotron Rad.* **22**, 187–190.
Debela, M., Magdolen, V., Grimminger, V., Sommerhoff, C. P., Messerschmidt, A., Huber, R., Friedrich, R., Bode, W. & Goettig, P. (2006). *J. Mol. Biol.* **362**, 1094–1107.
Debela, M., Magdolen, V., Schechter, N., Valachova, M., Lottspeich, F., Craik, C. S., Choe, Y., Bode, W. & Goettig, P. (2006). *J. Biol. Chem.* **281**, 25678–25688.
Emsley, P., Lohkamp, B., Scott, W. G. & Cowtan, K. (2010). *Acta Cryst.* D**66**, 486–501.
Hodel, A., Kim, S.-H. & Brünger, A. T. (1992). *Acta Cryst.* A**48**, 851–858.
Kabsch, W. (2010). *Acta Cryst.* D**66**, 125–132.
Lovell, S. C., Word, J. M., Richardson, J. S. & Richardson, D. C. (2000). *Proteins*, **40**, 389–408.
Matsumura, M., Bhatt, A. S., Andress, D., Clegg, N., Takayama, T. K., Craik, C. S. & Nelson, P. S. (2005). *Prostate*, **62**, 1–13.
McCoy, A. J., Grosse-Kunstleve, R. W., Adams, P. D., Winn, M. D., Storoni, L. C. & Read, R. J. (2007). *J. Appl. Cryst.* **40**, 658–674.
McPhillips, T. M., McPhillips, S. E., Chiu, H.-J., Cohen, A. E., Deacon, A. M., Ellis, P. J., Garman, E., Gonzalez, A., Sauter, N. K., Phizackerley, R. P., Soltis, S. M. & Kuhn, P. (2002). *J. Synchrotron Rad.* **9**, 401–406.
Nelson, P. S., Gan, L., Ferguson, C., Moss, P., Gelinas, R., Hood, L. & Wang, K. (1999). *Proc. Natl Acad. Sci. USA*, **96**, 3114–3119.
Olsson, M. H. M., Søndergaard, C. R., Rostkowski, M. & Jensen, J. H. (2011). *J. Chem. Theory Comput.* **7**, 525–537.
Prassas, I., Eissa, A., Poda, G. & Diamandis, E. P. (2015). *Nature Rev. Drug Discov.* **14**, 183–202.
Ramsay, A. J., Dong, Y., Hunt, M. L., Linn, M., Samaratunga, H., Clements, J. A. & Hooper, J. D. (2008). *J. Biol. Chem.* **283**, 12293–12304.
Riley, B. T., Ilyichova, O., Costa, M. G. S., Porebski, B. T., de Veer, S. J., Swedberg, J. E., Kass, I., Harris, J. M., Hoke, D. E. & Buckle, A. M. (2016). *Sci. Rep.* **6**, 35385.
Riley, B. T., Ilyichova, O., de Veer, S. J., Swedberg, J. E., Wilson, E., Hoke, D. E., Harris, J. M. & Buckle, A. M. (2019). *Biochemistry*, **58**, 2524–2533.
Swedberg, J. E., de Veer, S. J., Sit, K. C., Reboul, C. F., Buckle, A. M. & Harris, J. M. (2011). *PLoS One*, **6**, e19302.
Swedberg, J. E., Ghani, H. A., Harris, J. M., de Veer, S. J. & Craik, D. J. (2018). *ACS Med. Chem. Lett.* **9**, 1258–1262.
Swedberg, J. E., Nigon, L. V., Reid, J. C., de Veer, S. J., Walpole, C. M., Stephens, C. R., Walsh, T. P., Takayama, T. K., Hooper, J. D., Clements, J. A., Buckle, A. M. & Harris, J. M. (2009). *Chem. Biol.* **16**, 633–643.
Takayama, T. K., McMullen, B. A., Nelson, P. S., Matsumura, M. & Fujikawa, K. (2001). *Biochemistry*, **40**, 15341–15348.
Winn, M. D., Ballard, C. C., Cowtan, K. D., Dodson, E. J., Emsley, P., Evans, P. R., Keegan, R. M., Krissinel, E. B., Leslie, A. G. W., McCoy, A., McNicholas, S. J., Murshudov, G. N., Pannu, N. S., Potterton, E. A., Powell, H. R., Read, R. J., Vagin, A. & Wilson, K. S. (2011). *Acta Cryst.* D**67**, 235–242.
Yousef, G. M., Obiezu, C. V., Luo, L.-Y., Black, M. H. & Diamandis, E. P. (1999). *Cancer Res.* **59**, 4252–4256.